Three-dimensional computer simulations of feeding behaviour in red and giant pandas relate skull biomechanics with dietary niche partitioning

Borja Figueirido[1], Zhijie J. Tseng[2], Francisco J. Serrano-Alarcón[1], Alberto Martín-Serra[1] and Juan F. Pastor[3],

[1]Departamento de Ecología y Geología de la Facultad de Ciencias, Universidad de Málaga, 29071-Málaga, Spain.

[2]Division of Paleontology, American Museum of Natural History, Central Park West at 79th Street, New York 10024, U.S.A. jtseng@amnh.org

[3]Department of Anatomy and Radiology, Anatomical Museum, University of Valladolid, Spain.

The red (*Ailurus fulgens*) and giant (*Ailuropoda melanoleuca*) pandas are mammalian carnivores convergently adapted to a bamboo feeding diet. However, whereas *Ailurus* forages almost entirely on younger leaves, fruits and tender trunks, *Ailuropoda* relies more on trunks and stems. Such difference in foraging mode is considered a strategy for resource partitioning where they are sympatric. Here, we use finite-element analysis to test for mechanical differences and similarities in skull performance between *Ailurus* and *Ailuropoda* related to diet. Feeding simulations suggest that the two panda species have similar ranges of mechanical efficiency and strain energy profiles across the dentition, reflecting their durophagous diet. However, the stress distributions and peaks in the skulls of *Ailurus* and *Ailuropoda* are remarkably different for biting at all tooth locations. Although the skull of *Ailuropoda* is capable of resisting higher stresses than the skull of *Ailurus*, the latter is able to distribute stresses more evenly throughout the skull. These differences in skull biomechanics reflect their distinct bamboo feeding preferences. *Ailurus* uses repetitive chewing in an extended mastication to feed on soft leaves, and *Ailuropoda* exhibits shorter and more discrete periods of chomp-and-swallow feeding to break down hard bamboo trunks.

Keywords: FEA, biomechanics, feeding behaviour, *Ailurus*, *Ailuropoda,* resource partitioning

1. INTRODUCTION

Phenotypic similarity between the red (*Ailurus fulgens*) and giant (*Ailuropoda melanoleuca*) pandas is largely considered a remarkable example of evolutionary convergence among mammals [1], because they belong to different carnivoran families (Ailuridae and Ursidae, respectively [2]; electronic supplementary material, figure S1a) and have an unusual durophagous diet based on bamboo [3,4]. Accordingly, despite their different body mass (approx. 5 kg for *Ailurus* [3] and approx. 100 kg for *Ailuropoda* [4]), morphometric studies [5–8] have revealed shared morphological traits in their skulls (e.g. deep and concave mandibles with tall coronoid processes and brachycephalic crania with a highly vaulted calvarium and broad zygomatic arches) related to producing the required high bite forces for feeding on bamboo and to dissipate the generated stress [9].

Despite both having this unique diet among carnivores, the pandas differ in their foraging mode. *Ailurus* feeds almost entirely on younger leaves supplemented by fruits and peeled trunks [10], whereas *Ailuropoda* relies more on peeled trunks and stems of the same bamboo species, feeding with less discrimination of plant parts [11,12]. In fact, although *Ailurus* and *Ailuropoda* use different microhabitats [13], this difference in the parts of the bamboo plants consumed has been attributed as a strategy for resource partitioning [14] in areas where they coexist (electronic supplementary material, figure S1b). In this paper, we use finite-element analysis (FEA) to explore both the biomechanical basis for different foraging modes and indications of resource partitioning between *Ailurus* and *Ailuropoda* (see also [15]).

2. MATERIAL AND METHODS

Skulls of a red and a giant panda housed at the Anatomical Museum of Valladolid University (Spain) were CT-scanned using a Toshiba Aquilion (*Ailurus*/*Ailuropoda*: voltage: 120/120 kV; current: 250/250 mA; slice thickness: 0.5/0.5 mm; pixel spacing: 0.228/0.520 mm; image dimensions: 512 x 512 pixels). All images were exported in DICOM format. The CT images were processed in MIMICS (Materialise, Belgium), where surface reconstructions were generated (electronic supplementary material, figure S2). The surface models were then cleaned in MIMICS REMESH and GEOMAGIC STUDIO (Geomagic Inc., USA), with triangle element quality checked in STRAND v. 7 (Strand7 Pty Ltd, Australia). Final, error-free surface meshes were then solid-meshed with four-noded tetrahedral elements.

Muscle input forces and output bite forces were estimated using the dry-skull method (DSM) [16] from digital models in their original sizes (electronic supplementary material, figure S3 and table S3). Nodal constraints were placed at each of the left and right temporomandibular joints (TMJ) and at a given tooth position (electronic supplementary material, figure S2) to simulate jaw closure during biting. Muscle forces reflected differential activation between the working (biting) and balancing sides and were simulated using BONELOAD [17] (see the electronic supplementary material). All models were assigned Young's modulus of 20 GPa and Poisson's ratio of 0.3. All analyses were linear and static, simulating maximum jaw-closing muscle contraction.

A total of 222 FE analyses were conducted (electronic supplementary material, table S1) to analyse different mesh-density models of *Ailurus* (from approx. 950 k to approx. 2 million elements) and *Ailuropoda* (from 1 to 2.7 million elements) (electronic supplementary material, table S2). We used analyses with muscle forces proportional to surface area for comparisons of stresses in original-size models, and analyses of volume-standardized models (scaling the *Ailurus* model to the volume of *Ailuropoda*)

with the same input muscle forces (using those of *Ailuropoda*) for comparing total strain energy (SE) and mechanical efficiency (ME) of biting (ratio of output force to input force) ([18]; electronic supplementary material, table S3).

3. RESULTS

Bite force estimates using DSM predicted a range of 130–248 N for *Ailurus* and 539–1836 N for *Ailuropoda*; FEA bite forces of original-size models fell within these ranges and verify the validity of FE model input parameters (tables 1 and 2). The means of ME and SE (proxy for structural work-efficiency) values obtained from all cranium and mandible models of *Ailurus* and *Ailuropoda* are shown in tables 1 and 2.

Comparison between the models of both species showed similar SE values over a large range of ME across the dentition (tables 1 and 2). The two carnivoran species also have similar ranges of ME and profiles of non-uniform increase in ME across the dentition (figure 1a). However, the *Ailurus* models exhibit a slightly more mechanically efficient cranium from the third premolar (P3) to the second molar (M2) bite positions (figures 1a and 2a; x-axis). At the same time, SE values tend to be higher in *Ailurus* compared with *Ailuropoda*, indicating that higher ME in the former corresponds with a less work-efficient skull (figures 1a and 2a; y-axis). Comparison of maximum von Mises (VM, proxy for strength) stress shows that the cranium and the mandible of *Ailurus* are more stressed (i.e. lower strength) than the ones of *Ailuropoda* in all bite simulations (figures 1b and 2b). Furthermore, *Ailurus* exhibits a higher number of elements with higher VM stress relative to *Ailuropoda* (histograms in figures 1c–e and 2c–e). Accordingly, whereas *Ailurus* experiences higher peak stresses at the TMJ and the antorbital region on both sides of the skull during unilateral bites, *Ailuropoda* experiences more concentrated stresses in the rostrum (figures 1c–e and 2c–e).

Furthermore, the mandible and crania of *Ailurus* exhibit more evenly distributed stress in all bite simulations than the ones of *Ailuropoda* (histograms in figures 1c–e and 2c–e). This indicates that *Ailurus* models exhibit more elements with intermediate values of stress than *Ailuropoda* models, which contain more elements with relatively low stresses.

4. DISCUSSION

Our analyses indicate that *Ailurus* and *Ailuropoda* have similar skull performance (tables 1 and 2), which probably reflects the high biomechanical demands imposed by feeding on tough bamboo and indicates that both panda skulls have relatively invariant work-efficiency (measured by SE) across different biting positions. These differences relate to several morphological adaptations permitting exertion of high bite forces required for feeding on bamboo and for dissipating the stresses generated (e.g. short-snouted skull with a dome-like frontal region, and enlarged areas for the attachment of masticatory muscles [7,9]). These morphological features manifest in stiff skulls that exhibit a capacity to bite at all tooth positions while keeping SE relatively invariant (figures 1 and 2).

Comparative FEA also reveals some biomechanical differences associated with diet between the pandas: whereas the mandible of *Ailurus* has comparable ME as *Ailuropoda*, the cranium of the former has higher ME at corresponding P3-M2 tooth positions than *Ailuropoda* (figures 1a and 2a). This is associated with longer masseter input lever arms of *Ailurus* relative to *Ailuropoda*. By contrast, both the cranium and the mandible of *Ailuropoda* experience lower values of maximum VM stress (figures 1b and 2b) than the one of *Ailurus*. This difference in skull performance probably reflects the hard bamboo trunks consumed by *Ailuropoda* relative to the soft leaves regularly

consumed by *Ailurus*, which in turn is associated with a shallower mandibular body and the lesser paranasal sinuses of *Ailurus* relative to *Ailuropoda* [7,9]. Therefore, both morphological and biomechanical data indicate that the skull of *Ailurus* is weaker than the one of *Ailuropoda*. By contrast, stress in both the cranium and the mandible of *Ailurus* is more evenly distributed than in *Ailuropoda* (figures 1c–e and 2c–e), which could reflect an adaptation of *Ailurus* to use repetitive chewing during prolonged periods as higher frequency of mastication cycles places more repetitive stress on the craniodental system [19].

Therefore, although both pandas have an exceptional ability for exerting large bite forces and to dissipate the stress generated, they use this ability in different ways. The skull of *Ailuropoda* is more capable of exerting high peak forces to break bamboo trunks and stems, and to resist the stresses generated, during short and discrete periods of time. In comparison, the skull shape of *Ailurus* is better able to resist fatigue as a result of constant chewing applying submaximal forces over protracted periods of time by distributing stress more evenly. Our results provide mechanistic bases of dietary differences and niche partitioning between the pandas, offering a more fundamental understanding of the biomechanical factors that permit species coexistence in sympatry.

ACKNOWLEDGEMENTS

Z.J.T. thanks J. Flynn for mentorship and research resources. J.F.P. thanks J.M. Montes for scanning facilities. We are specially grateful to Dr Lautenschlager and one anonymous reviewer for their insightful comments.

DATA ACCESSIBILITY.

Data deposited in the Dryad repository: doi:10.5061/dryad.8n8v3.

FUNDING STATEMENT.

This research was supported by a MINECO-grant (B.F.; CGL2012-37866) and a Frick Postdoctoral Fellowship (Z.J.T.).

REFERENCES

1. Gittleman JL. 1994 Are the pandas successful specialists or evolutionary failures? BioScience 44, 456–464. (doi:10.2307/1312297)

2. Flynn JJ, Finarelli JA, Zehr S, Hsu J, Nedbal M. 2005 Molecular phylogeny of the Carnivora (Mammalia): assessing the impact of increased sampling on resolving enigmatic relationships. Syst. Biol. 54, 317–337. (doi:10.1080/10635150590923326)

3. Chorn J, Hoffmann RS. 1978 *Ailuropoda melanoleuca*. Mamm. Spec. 110, 1–6 (doi:10. 2307/3503982)

4. Roberts MS, Gittleman JL. 1984 *Ailurus fulgens*. Mamm. Spec. 222, 1–8. (doi:10.2307/3503840)

5. Figueirido B, Serrano-Alarcón FJ, Slater GJ, Palmqvist P. 2010 Shape at the cross-roads: homoplasy and history in the evolution of the carnivoran skull towards herbivory. J. Evol. Biol. 23, 2579–2594. (doi:10.1111/j.1420-9101.2010.02117.x)

6. Davis DD. 1964 The giant panda: a morphological study on evolutionary mechanisms. Fieldiana Geol. 3, 1–339.

7. Figueirido B, Serrano-Alarcón FJ, Palmqvist P. 2012 Geometric morphometrics shows differences and similarities in skull shape between the red and giant pandas. J. Zool. 286, 293–302. (doi:10.1111/j.1469-7998.2011.00879.x)

8. Zhang S, Pan R, Li M, Oxnard C, Wei F. 2007 Mandible of the giant panda (*Ailuropoda melanoleuca*) compared with Chinese carnivores: functional adaptation. Biol. J. Linn. Soc. 92, 449–456. (doi:10.1111/j.1095-8312.2007.00876.x)

9. Figueirido B, Tseng ZJ, Martín-Serra A. 2013 Skull shape evolution in durophagous carnivorans. Evolution 67, 1975–1993. (doi:10.1111/evo.12059)

10. Reid DG, Hu J, Huang Y. 1991 Ecology of the red panda in Wolong Reserve, China. J. Zool. 225, 347–364. (doi:10.1111/j.1469-7998.1991.tb03821.x)

11. Schaller GB. 1993 The last panda. Chicago, IL: University of Chicago Press.

12. Huang X, Zhang Z. 2008 Comparison of ecological traits between giant panda and red panda: the effects of food, body size, and phylogenesis. Sichuan J. Zool. 27, 687–692.

13. Wei F, Feng Z, Wang Z, Hu J. 2000 Habitat use and separation between the giant panda and the red panda. J. Mammal. 80, 448–455. (doi:10.1644/1545-1542(2000)081,0448:HUASBT.2.0.CO;2)

14. Wei F, Feng Z, Wang Z, Li M. 1999 Feeding strategy and resource partitioning between giant and red pandas. Mammalia 63, 417–430 (doi:10.1515/mamm.1999.63.4.417)

15. Oldfield CC, McHenry CR, Clausen PD, Chamoli U, Parr WCH, Stynder DD, Wroe S. 2012 Finite element analysis of ursid cranial mechanics and the prediction of feeding behaviour in the extinct giant Agriotherium africanum. J. Zool. 286, 171. (doi:10.1111/j.1469-7998.2011.00862.x)

16. Thomason JJ. 1991 Cranial strength in relation to estimate biting forces in some mammals. Can. J. Zool. 69, 2326–2333. (doi:10.1139/z91-327)

17. Grosse I, Dumont ER, Coletta C, Tolleson A. 2007 Techniques for modeling muscle-induced forces in finite element models of skeletal structures. Anat. Rec. 290, 1069–1088 (doi:10.1002/ar.20568)

18. Dumont ER, Grosse IR, Slater GJ. 2009 Requirements for comparing the performance of finite element models of biological structures. J. Theor. Biol. 256, 96–103. (doi:10.1016/j.jtbi.2008.08.017)

19. Williams SH, Stover KK, Davis JS, Stephane JM. 2011 Mandibular corpus bone strains during mastication in goats (Capra hircus): a comparison of ingestive and rumination chewing. Arch. Oral Biol. 56, 960–971. (doi:10.1016/j.archoralbio.2011.02.014)

Table 1. Cranium analysis showing bite forces calculated by DSM and FEA (original-size/volume-scaled *Ailurus*) both in Newtons (N); mechanical efficiency (ME); total SE in joules (J) for the volume-scaled models and maximum VM stress in megapascal (MPa) from 98% of VM stress values in original-sized models with muscle forces scaled to surface area in both pandas. Data shown in the electronic supplementary material, tables S4–S7.

	tooth position	DSM bite force (N)	FEA bite force (N)	ME	strain energy (J)	max. VM stress (MPa)
A. melanoleuca	C	667.8	672.36	0.1487	0.0915	4.07
	P2	748.96	799.42	0.1768	0.1014	4.44
	P3	809.91	853.71	0.1888	0.0993	4.29
	P4	953.7	1020.35	0.2256	0.0978	4.3
	M1	1179.85	1243.37	0.275	0.1225	4.32
	M2	1593.26	1710.3	0.3782	0.1685	4.32
A. fulgens	C	135.91	111.83/786.62	0.1657/0.1740	0.1377	7.91
	P2	148.86	138.11/674.79	0.2046/0.1492	0.1347	7.6
	P3	158.68	136.43/974.82	0.2021/0.2156	0.1341	7.4
	P4	177.28	164.89/1214.68	0.2443/0.2687	0.152	7.14
	M1	209.8	194.79/1386.92	0.2886/0.3068	0.1498	7.4
	M2	238.62	180.61/1842.59	0.2676/0.4075	0.2203	8.51

Table 2. Mandible analysis showing bite forces calculated by DSM and FEA (original-size/volume-scaled *Ailurus*) both in Newtons (N); mechanical efficiency (ME); total SE in joules (J) for the volume-scaled models and maximum VM stress in megapascal (MPa) from 98% of VM stress values in original-sized models with muscle forces scaled to surface area in both pandas. Data shown in the electronic supplementary material, tables S4–S7.

	tooth position	DSM bite force (N)	FEA bite force (N)	ME	strain energy (J)	max. VM stress (MPa)
A. melanoleuca	c	639.18	1028.89	0.2276	0.4622	21.5
	p2	727.42	1141.69	0.2525	0.4396	22.8
	p3	788.35	1223.78	0.2707	0.4203	20.3
	p4	888.77	1311.62	0.2901	0.4095	21.7
	m1	1112.8	1462.52	0.3235	0.3989	21.3
	m2	1453.97	2004.63	0.4434	0.4701	21.5
	m3	1836.71	2581.14	0.5709	0.4109	11.3
A. fulgens	c	130.79	143.22/970.81	0.2122/0.2147	0.1377	7.91
	p2	146.07	164.45/1112.49	0.2437/0.2461	0.1347	7.6
	p3	161.13	179.88/1212.18	0.2665/0.2681	0.1341	7.4
	p4	178.49	188.06/1323.99	0.2787/0.2928	0.152	7.14
	m1	207.61	208.68/1507.29	0.3092/0.3334	0.1498	7.4
	m2	247.5	281.79/1886.39	0.4175/0.4172	0.2203	8.51

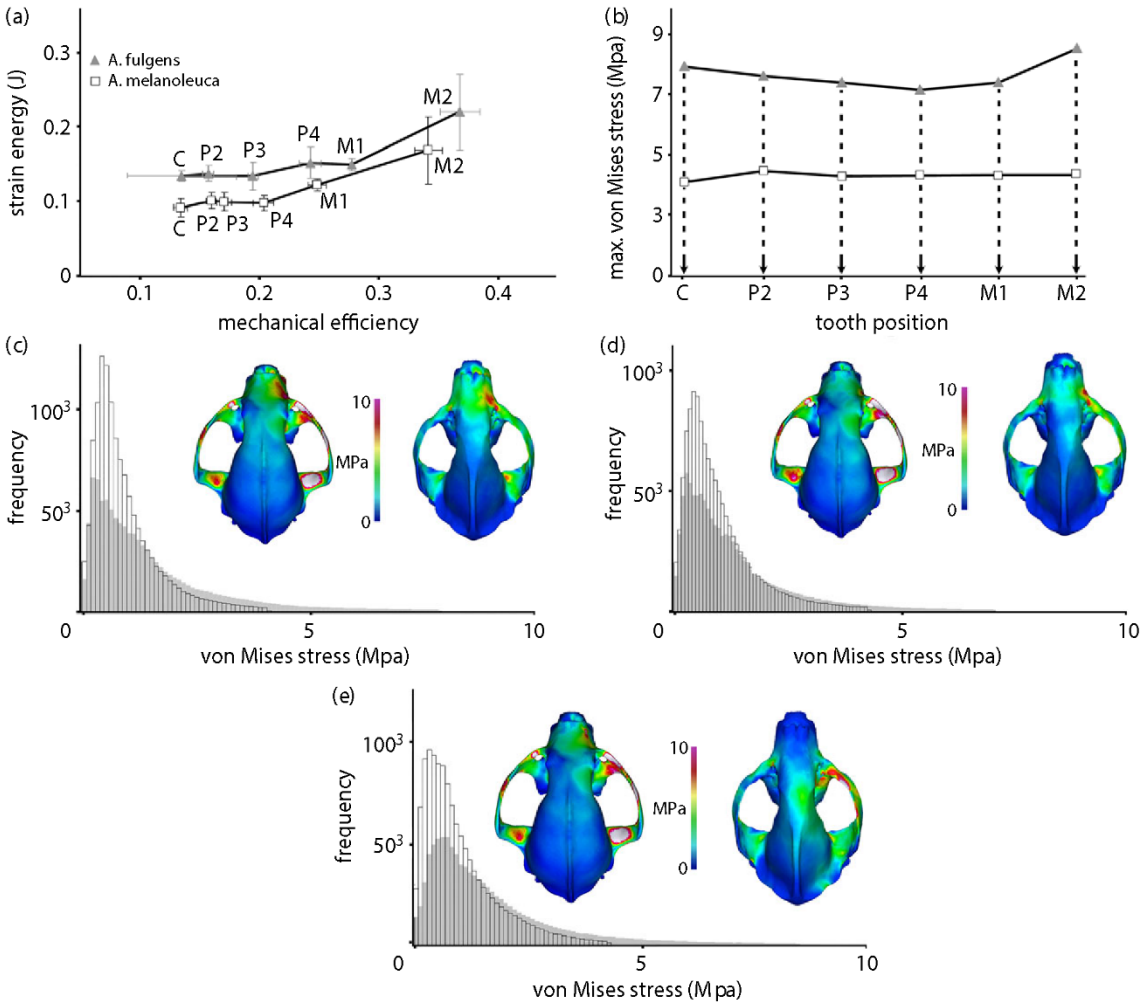

1

2 **Figure 1.** (a) ME on SE of *Ailurus* (volume-scaled) and *Ailuropoda* cranium models.
3 The grand mean of all resolution models is shown; (b) mean maximum VM stress for
4 each simulated bite in the original-size models; (c–e) histograms (grey, *Ailurus*; white,
5 *Ailuropoda*) showing the frequency of elements to a given value of VM stress and
6 dorsal view of VM stress distribution in the original-size *Ailurus* (left) and *Ailuropoda*
7 (right) models for the bite simulated at the canine (c), fourth premolar (d) and second
8 molar (e). The maximum on the scale is 10 MPa. All results are for unilateral bites using
9 the right side of the dentition. Model results scaled to identical length. See also the
10 electronic supplementary material, figure S4.

11

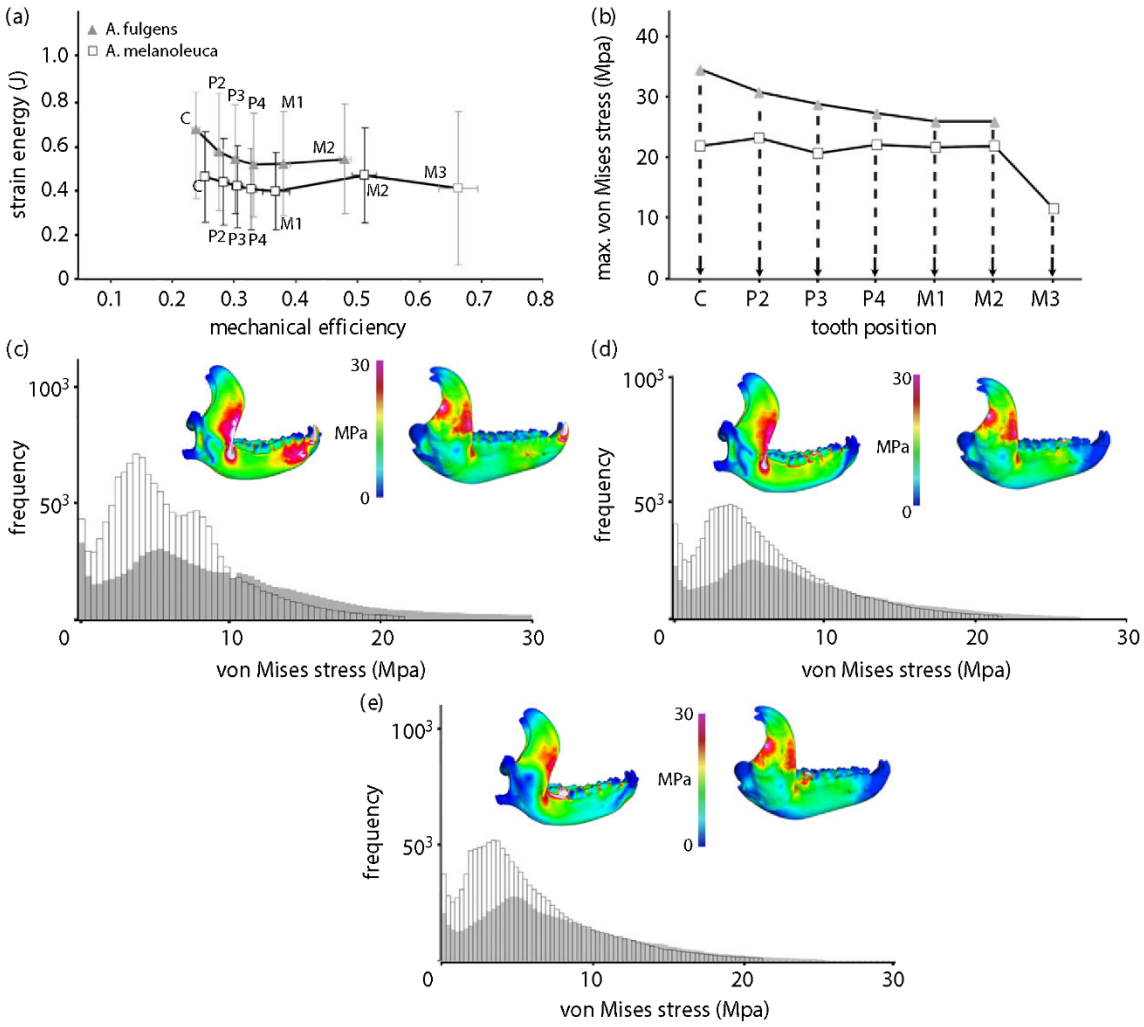

Figure 2. (a) ME on SE of *Ailurus* (volume-scaled) and *Ailuropoda* mandible models. The grand mean of all resolution models is shown; (b) mean maximum VM stress for each simulated bite in the original-size models; (c–e) histograms (grey, *Ailurus*; white, *Ailuropoda*) showing the frequency of elements following [18] to a given value of VM stress and dorsal view of VM stress distribution in the original-size *Ailurus* (left) and *Ailuropoda* (right) models for the bite simulated at the canine (c), fourth premolar (d) and second molar (e). The maximum on the scale is 30 MPa. All results are for unilateral bites using the right side of the dentition. Model results scaled to identical length. See also the electronic supplementary material, figure S5.